Bioconjugate Chemistry

Article

pubs.acs.org/bc

Impact of Boronate Capping Groups on Biological Characteristics of Novel ^{99m}Tc(III) Complexes [^{99m}TcCl(CDO)(CDOH)$_2$B-R] (CDOH$_2$ = Cyclohexanedione Dioxime)

Yong Yang,[†,‡] Yumin Zheng,[§] Elena Tomaselli,[‡] Wei Fang,*[,†] and Shuang Liu*[,‡]

[†]Department of Nuclear Medicine, Cardiovascular Institute & Fu Wai Hospital, Chinese Academy of Medical Science & Peking Union Medical College, Beijing 100037, China

[‡]School of Health Sciences, Purdue University, West Lafayette, Indiana 47907, United States

[§]Department of Nuclear Medicine, China-Japan Friendship Hospital, Beijing 100029, China

Supporting Information

ABSTRACT: This study sought to explore the impact of boronate groups on the heart uptake and myocardial retention of novel ^{99m}Tc(III) complexes [^{99m}TcCl(CDO)(CDOH)$_2$B-R] (^{99m}Tc-ISboroxime: R = isoxazol-4-yl (IS); ^{99m}Tc-MPboroxime: R = *N*-methylpyridinium (MP); ^{99m}Tc-PAboroxime: R = pyrazol-3-yl (PA); ^{99m}Tc-PYboroxime: R = pyridin-3-yl (PY); and ^{99m}Tc-5Uboroxime: R = uracil-5-yl (5U)). All five new ^{99m}Tc(III) radiotracers were prepared in high yield and high radiochemical purity (RCP = 90−98%), and they remained stable in the kit mixture for >6 h. Biodistribution and imaging (planar and SPECT) studies were carried out using Sprague−Dawley (SD) rats. Planar image quantification was performed to compare their myocardial retention and liver clearance kinetics. It was found that their heart retention and liver clearance curves were best fitted to the biexponential decay function. The initial heart uptake at 0−1 min after injection followed the general ranking order of ^{99m}Tc-ISboroxime (4.98 ± 1.05%ID) ~ ^{99m}Tc-Teboroxime (4.56 ± 0.91%ID) ~ ^{99m}Tc-PAboroxime (4.03 ± 1.23%ID) ~ ^{99m}Tc-PYboroxime (4.07 ± 0.80% ID) > ^{99m}Tc-5Uboroxime (3.24 ± 0.67%ID) > ^{99m}Tc-MPboroxime (2.53 ± 0.65%ID). The fast-phase myocardial retention time followed the general order of ^{99m}Tc-PAboroxime (3.21 ± 0.29 min) > ^{99m}Tc-Teboroxime (1.63 ± 0.40 min) ~ ^{99m}Tc-PYboroxime (1.57 ± 0.29 min) ~ ^{99m}Tc-ISboroxime (1.55 ± 0.32 min) > ^{99m}Tc-MPboroxime (0.68 ± 0.16 min) > ^{99m}Tc-5Uboroxime (0.33 ± 0.11 min). ^{99m}Tc-PAboroxime (3.05 ± 1.10%ID/g) and ^{99m}Tc-ISboroxime (3.75 ± 0.68%ID/g) had the 2 min initial heart uptake very close to that of ^{99m}Tc-Teboroxime (3.30 ± 0.50%ID/g). However, the myocardial retention time of ^{99m}Tc-PAboroxime was significantly longer than that of ^{99m}Tc-ISboroxime and ^{99m}Tc-Teboroxime. Even though the best time window is 0−5 min for SPECT image acquisition, high quality SPECT images could be obtained during the first 30 min postinjection of ^{99m}Tc-PAboroxime in SD rats. This statement was supported by the SPECT/CT studies in normal pigs. On the basis of results from this study, it was concluded that boronate groups had significant impact on the heart uptake, myocardial retention, and liver clearance kinetics of ^{99m}Tc(III) complexes [^{99m}TcCl(CDO)(CDOH)$_2$B-R]. The combination of high initial heart uptake with longer myocardial retention makes it possible to image the heart with ^{99m}Tc-PAboroxime during the first 30 min using both standard and specialized cardiac SPECT cameras.

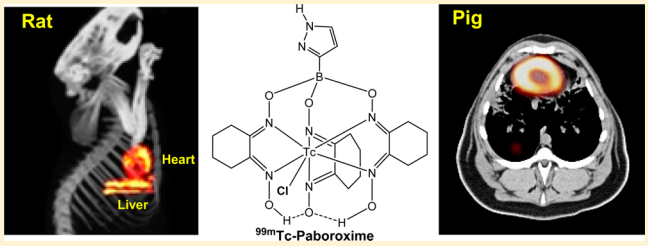

INTRODUCTION

Myocardial perfusion imaging (MPI) with SPECT (single photon-emission computed tomography) is an integral component in evaluation of the patients with known or suspected coronary artery disease (CAD),[1−9] and remains the only imaging modality available for assessment of physiological consequences of coronary stenosis or myocardial infarction.[9] Over the past two decades, the overwhelming success of SPECT MPI is largely due to the widespread nuclear cardiology applications of ^{99m}Tc-Sestamibi ([^{99m}Tc(MIBI)$_6$]$^+$: MIBI = 2-methoxy-2-methylpropylisonitrile) and ^{99m}Tc-Tetrofosmin ([^{99m}TcO$_2$(tetrofosmin)$_2$]$^+$: tetrofosmin = 1,2-bis[bis(2-ethoxyethyl)phosphino]ethane)). SPECT MPI will continue to play a major role in nuclear cardiology for many years ahead.[6]

Precise measurement of the regional blood flow has significant clinical importance in identifying ischemia, defining the extent and severity of disease, assessing the myocardial viability, establishing the need for surgical intervention, and monitoring the effects of treatment in the patients with known or suspected CAD. A significant drawback of ^{99m}Tc-Sestamibi and ^{99m}Tc-Tetrofosmin is their low first-pass extraction fractions and the lack of linear relationship between their

Received: December 10, 2014
Revised: January 8, 2015
Published: January 13, 2015

DOI: 10.1021/bc500583k
Bioconjugate Chem. 2015, 26, 316−328

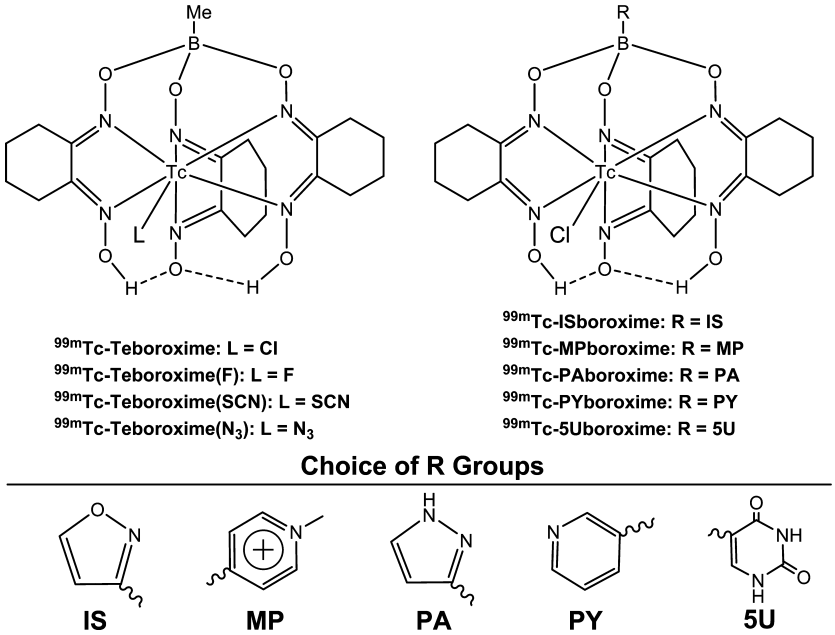

Figure 1. Chemdraw structures of new ^{99m}Tc(III) radiotracers [^{99m}TcCl(CDO)(CDOH)$_2$B-R] (R = IS, MP, PA, PY, and 5U) evaluated in this study for their potential as heart imaging agents.

heart uptake and regional blood flow at >2.5 mL/min/g,[3−6] which reduces their clinical values for quantification of the blood flow. In contrast, ^{99m}Tc-Teboroxime (Figure 1: [^{99m}TcCl(CDO)(CDOH)$_2$BMe], and $CDOH_2$ = cyclohexanedione dioxime) is the first FDA-approved ^{99m}Tc radiotracer for MPI, and has the highest first-pass extraction fraction among all ^{99m}Tc perfusion radiotracers.[10−12] The high first-pass extraction fraction and linear relationship between its heart uptake and regional blood flow over a wide range (0−4.5 mL/min/g) permit accurate detection of CAD and precise delineation of perfusion defects, which is of considerable benefit for the patients with known or suspected CAD.[1−4,7] Despite this advantage, early clinical experiences were disappointing because of its short heart residence time and high liver uptake.[13−18] As a matter of fact, more than 60% of the initial heart radioactivity is washed out within 5 min after administration of ^{99m}Tc-Teboroxime,[12] which is too fast for the standard SPECT cameras to acquire high-quality heart images. Due to the tremendous developments in high-speed semiconductor cardiac SPECT cameras and the computer software for quantification of regional blood flow,[19−26] ^{99m}Tc-Teboroxime has been suggested as the candidate for SPECT MPI in the future.[27,28]

Previously, we reported ^{99m}Tc(III) complexes [^{99m}Tc(L)(CDO)(CDOH)$_2$B-Me] (Figure 1: ^{99m}Tc-Teboroxime, L = Cl; ^{99m}Tc-Teboroxime(F), L = F; ^{99m}Tc-Teboroxime(SCN), L = SCN; and ^{99m}Tc-Teboroxime(N_3), L = N_3) for their potential as heart imaging agents.[29] Among the five ^{99m}Tc(III) complexes evaluated in Sprague−Dawley (SD) rats, ^{99m}Tc-Teboroxime(N_3) had significantly longer myocardial retention than ^{99m}Tc-Teboroxime; but its initial heart uptake was much lower.[29] Both ^{99m}Tc-Teboroxime and ^{99m}Tc-Teboroxime(N_3) have a prolonged liver uptake, which will have a detrimental effect on the interpretation of heart radioactivity and accurate diagnosis of heart diseases, such as CAD.[1−10,30−32]

To overcome the shortcomings associated with ^{99m}Tc-Teboroxime, we prepared five new ^{99m}Tc(III) complexes [^{99m}TcCl(CDO)(CDOH)$_2$B-R] (Figure 1: ^{99m}Tc-ISboroxime: R = isoxazol-4-yl; ^{99m}Tc-MPboroxime: R = *N*-methylpyridinium; ^{99m}Tc-PAboroxime: R = pyrazol-3-yl; ^{99m}Tc-PYboroxime: R = pyridin-3-yl; and ^{99m}Tc-5Uboroxime: R = uracil-5-yl). In the literature,[33,34] the boronate caps in ^{99m}Tc(III) complexes [^{99m}TcCl(CDO)(CDOH)$_2$B-R] were mostly aliphatic groups because aromatics often result in ^{99m}Tc radiotracers with higher lipophilicity, leading to higher liver uptake and lower heart/liver ratios. In this study, we used IS and PA because they both contain two two-heteroatoms (imine-N, isoxazol-O, or pyrazol-N), which are expected to counterbalance the increased lipophilicity due to the extra carbon atoms. The MP and PY groups were of our interest since they carry different molecular charges. The 5U group was our choice due to its higher hydrophilicity. This study was specifically designed to explore the impact of boronate-capping groups on the heart uptake, myocardial retention, and liver clearance kinetics of new ^{99m}Tc(III) radiotracers. The main objective is to maximize the myocardial retention and minimize the liver radioactivity accumulation while maintaining the high heart uptake. The combination of high heart uptake and long myocardial retention will make it possible to use them for MPI studies with both standard and specialized cardiac SPECT cameras.

RESULTS

Radiochemistry. New ^{99m}Tc(III) complexes [^{99m}TcCl(CDO)(CDOH)$_2$B-R] (Figure 1: R = IS, MP, PA, PY, and 5U) were prepared using literature methods.[29,34] Radiolabeling was completed by heating the reaction mixture at 100 °C for 10−15 min. Their RCP values were 90−98% (without postlabeling chromatographic purification) depending on the borate-capping group. They were all stable in reaction solution for >6 h at room temperature. It is very interesting to note that ^{99m}Tc-ISboroxime, ^{99m}Tc-MPboroxime, and ^{99m}Tc-PAboroxime all showed a small radiometric peak at 4−5 min (Figure 2) due to the ^{99m}Tc-species containing no boronate cap. We also found that it was possible to minimize the amount of this ^{99m}Tc-species with larger amount of boronic acid in each vial.

DOI: 10.1021/bc500583k
Bioconjugate Chem. 2015, 26, 316−328

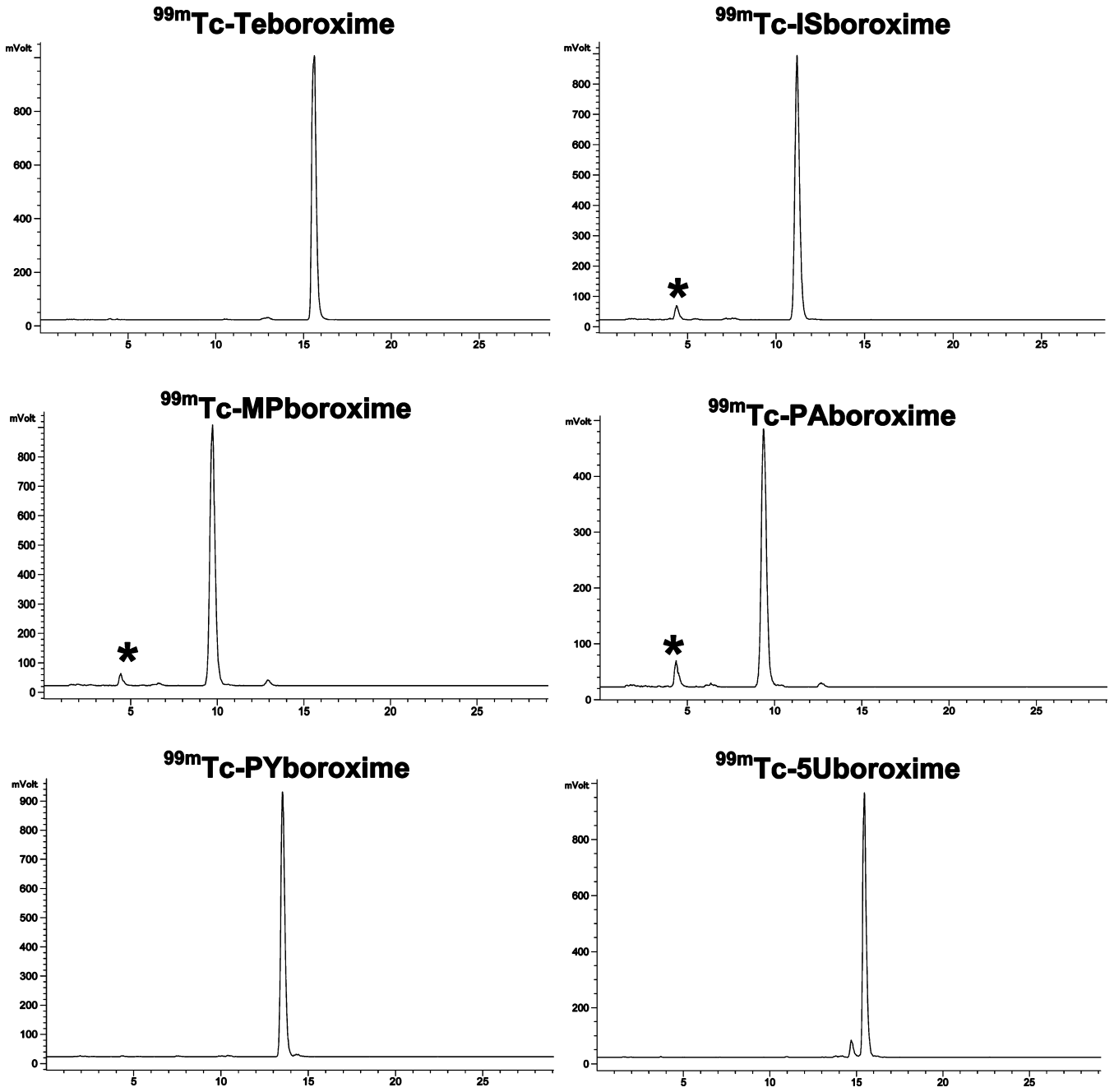

Figure 2. Representative radio-HPLC chromatograms for ^{99m}Tc-ISboroxime (RCP = 92−94%), ^{99m}Tc-MPboroxime (RCP = 93−95%), ^{99m}Tc-PAboroxime (RCP = 90−93%), and ^{99m}Tc-Uboroxime (RCP = 94−96%). ^{99m}Tc-Teboroxime (RCP >95%) was used only for comparison purposes. The radiometric peak at 4−5 min is from a ^{99m}Tc-species without the boronate-capping group.

However, more boronic acid often led to the formation of other radioimpurities.

Dynamic Planar Imaging. Planar imaging studies (Figure 3) were performed on five new radiotracers [^{99m}TcCl(CDO)-$(CDOH)_2$B-R] (R = IS, MP, PA, PY, and 5U) in the SD rats under anesthesia to compare their heart retention and liver clearance kinetics. The purpose of these studies was to select appropriate ^{99m}Tc radiotracers for biodistribution. Image quantification data were summarized in Table 1 to compare their initial %ID heart uptake and myocardial retention times. The heart retention curves were best fitted to a biexponential function (Figure 4). In general, the planar images acquired at 0−1 min using ^{99m}Tc-ISboroxime, ^{99m}Tc-PAboroxime, and ^{99m}Tc-PYboroxime all had a high initial heart uptake. The initial heart uptake followed the ranking order of ^{99m}Tc-ISboroxime (4.98 ± 1.05%ID) ~ ^{99m}Tc-Teboroxime (4.56 ± 0.91%ID) ~ ^{99m}Tc-PAboroxime (4.03 ± 1.23%ID) > ^{99m}Tc-PYboroxime (4.07 ± 0.80%ID) > ^{99m}Tc-5Uboroxime (3.24 ± 0.67%ID) > ^{99m}Tc-MPboroxime (2.53 ± 0.65%ID). Like ^{99m}Tc-Teboroxime, all new ^{99m}Tc(III) radiotracers had a significant myocardial washout. The fast-phase myocardial retention time followed the general ranking order of ^{99m}Tc-PAboroxime (3.21 ± 0.29 min) > ^{99m}Tc-Teboroxime (1.63 ± 0.40 min) ~ ^{99m}Tc-PYboroxime (1.57 ± 0.29 min) ~ ^{99m}Tc-ISboroxime (1.55 ± 0.32 min) > ^{99m}Tc-MPboroxime (0.68 ± 0.16 min) > ^{99m}Tc-5Uboroxime (0.33 ± 0.11 min). Approximately two-thirds of heart

DOI: 10.1021/bc500583k
Bioconjugate Chem. 2015, 26, 316−328

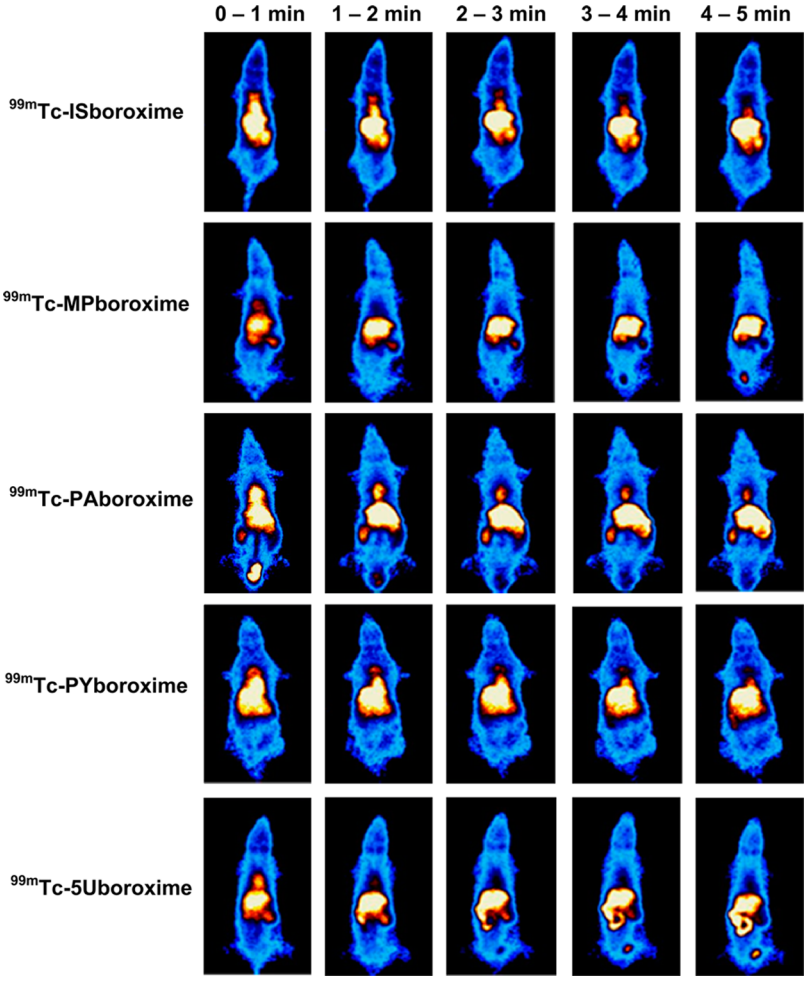

Figure 3. Representative planar images of the SD rats administered with ^{99m}Tc-ISboroxime, ^{99m}Tc-MPboroxime, ^{99m}Tc-PAboroxime, ^{99m}Tc-PYboroxime, and ^{99m}Tc-5Uboroxime over the first 5 min p.i. Each animal was injected with 1.0−1.5 mCi of ^{99m}Tc radiotracer. Arrows indicate the presence of heart. The radioactivity accumulation above the heart (in the white circle) was found in the blood vessels around the heart.

Table 1. Image Quantification Data to Compare Myocardial Retention Times of ^{99m}Tc-Teboroxime and ^{99m}Tc(III) Radiotracers [^{99m}TcCl(CDO)(CDOH)$_2$B-R] (R = IS, MP, PA, 3PY, and 5U)[a]

radiotracer	initial heart uptake (%ID)	fast phase half-life (min)	slow phase half-life (min)
^{99m}Tc-Teboroxime	4.56 ± 0.91	1.63 ± 0.40	60.7 ± 8.9
^{99m}Tc-ISboroxime	4.98 ± 1.50	1.55 ± 0.32	56.5 ± 10.6
^{99m}Tc-MPboroxime	2.53 ± 0.65	0.68 ± 0.16	56.2 ± 6.4
^{99m}Tc-PAboroxime	4.36 ± 0.93	3.21 ± 0.29	94.11 ± 27.71
^{99m}Tc-3PYboroxime	4.07 ± 0.80	1.57 ± 0.29	68.3 ± 16.0
^{99m}Tc-Uboroxime	3.24 ± 0.67	0.33 ± 0.11	27.3 ± 8.6

[a]Initial heart uptake was expressed as the %ID at 0−1 min p.i.

radioactivity cleared within 30 min for ^{99m}Tc-PAboroxime. The heart radioactivity disappeared by 2 min postinjection (p.i.) in the SD rats administered with ^{99m}Tc-MPboroxime or ^{99m}Tc-5Uboroxime. Apparently, the boronate capping groups had a significant impact on both the heart uptake and myocardial retention.

The liver clearance curves were also best fitted to the two-phase biexponential function (Figure 5). It must be noted that the liver radioactivity was expressed as the percentage of initial uptake (not the absolute values). The liver radioactivity accumulation of ^{99m}Tc-PAboroxime peaked at ∼3 min p.i., but its clearance kinetics was very similar to that of ^{99m}Tc-Teboroxime at >5 min p.i. ^{99m}Tc-ISboroxime had an initial liver uptake comparable to that of ^{99m}Tc-Teboroxime (Figure 4), and its liver radioactivity accumulation remained relatively unchanged over a 60 min study period. ^{99m}Tc-PYboroxime had a higher liver uptake than ^{99m}Tc-Teboroxime (Figure 3), and its liver clearance was slower (Figure 5). ^{99m}Tc-5Uboroxime showed a faster liver washout than other radiotracers evaluated in this study, most likely due to hydrophilicity of 5U moiety. There was a prolonged radioactivity accumulation above the heart in SD rats administered with ^{99m}Tc-ISboroxime and ^{99m}Tc-PYboroxime, but it was not quite obvious with ^{99m}Tc-PAboroxime (Figure 4).

Biodistribution. Tables 2 and 3 listed selected biodistribution data of ^{99m}Tc-PAboroxime and ^{99m}Tc-ISboroxime, respectively, in the SD rats. We were interested in these two radiotracers because they had the heart retention comparable to or better than ^{99m}Tc-Teboroxime (Figure 3). We found that they had similar blood radioactivity levels over the 60 min study period with ^{99m}Tc-Teboroxime.[29] The lung uptake of ^{99m}Tc-PAboroxime (1.80 ± 0.45, 0.88 ± 0.18, 0.68 ± 0.15, and 0.32 ± 0.08%ID/g at 2, 15, 30, and 60 min p.i., respectively) was significantly ($p < 0.01$) lower than that of ^{99m}Tc-ISboroxime (2.34 ± 0.93, 1.27 ± 0.33, 1.59 ± 0.76, and 0.88 ± 0.47%ID/g

DOI: 10.1021/bc500583k
Bioconjugate Chem. 2015, 26, 316−328

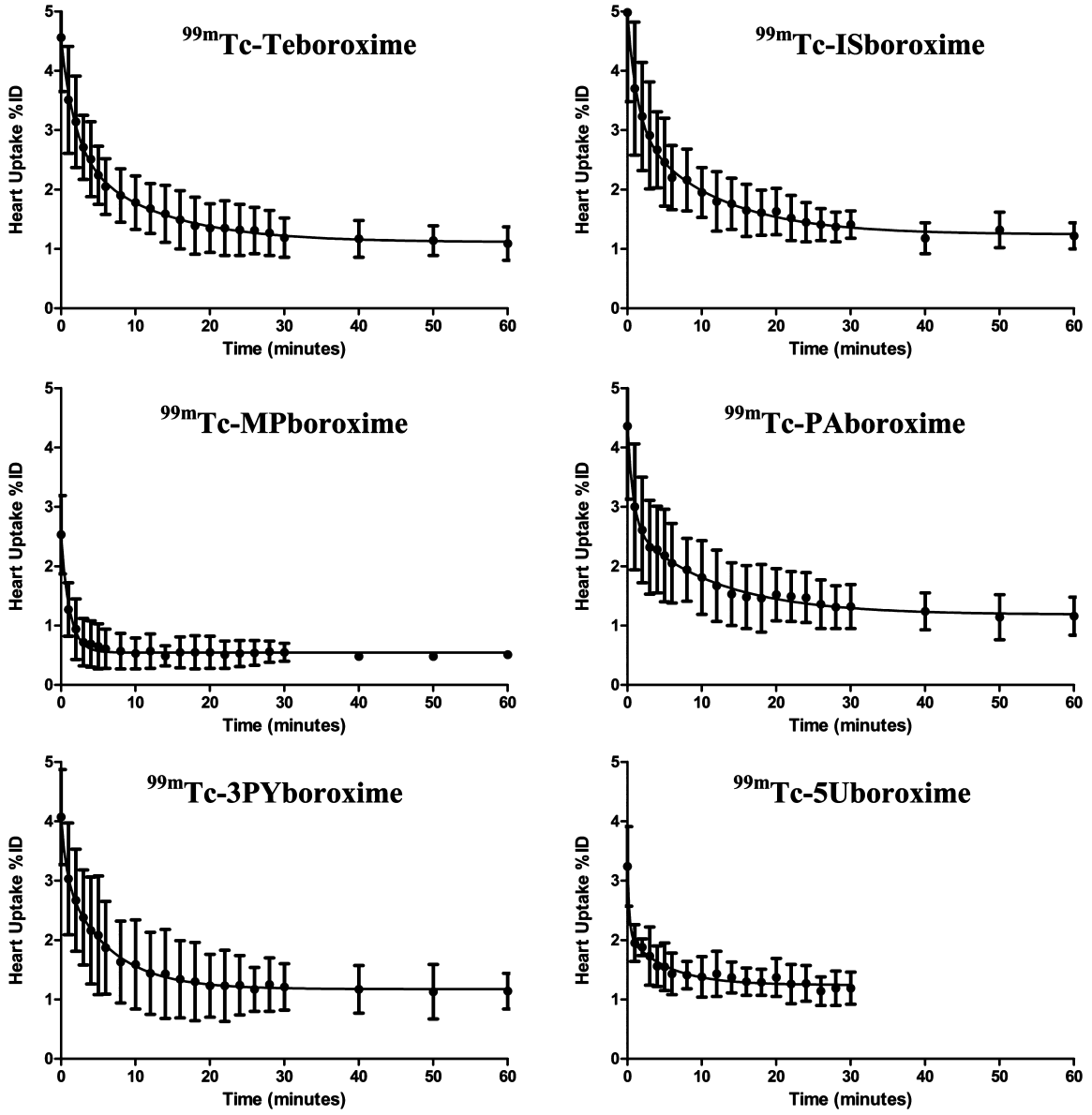

Figure 4. Image quantification data to compare the heart retention times of ^{99m}Tc-Teboroxime, ^{99m}Tc-ISboroxime, ^{99m}Tc-MPboroxime, ^{99m}Tc-PAboroxime, ^{99m}Tc-PYboroxime, and ^{99m}Tc-5Uboroxime over the first 5 min postinjection. The experimental data were expressed as the total heart uptake (%ID). The heart retention curve was best fitted to a biexponential function using the individual animal time/activity data.

at 2, 15, 30, and 60 min p.i., respectively) and ^{99m}Tc-Teboroxime (2.90 ± 0.35, 1.64 ± 0.28, 1.41 ± 0.25, and 0.94 ± 0.25%ID/g at 2, 15, 30, and 60 min p.i., respectively). ^{99m}Tc-PAboroxime had the initial heart uptake value (3.05 ± 1.01% ID/g at 2 min p.i.) almost identical to that of ^{99m}Tc-ISboroxime (3.75 ± 0.68%ID/g at 2 min p.i.) and ^{99m}Tc-Teboroxime (3.00 ± 0.37%ID/g at 2 min p.i.). However, the heart retention time of ^{99m}Tc-PAboroxime (heart uptake: 2.22 ± 0.17, 1.59 ± 0.14, and 0.89 ± 0.19%ID/g at 15, 30, and 60 min p.i., respectively) was significantly longer than that of both ^{99m}Tc-Teboroxime (heart uptake: 1.25 ± 0.09, 0.86 ± 0.17, and 0.58 ± 0.04%ID/g at 15, 30, and 60 min p.i., respectively) and ^{99m}Tc-ISboroxime (heart uptake: 1.68 ± 0.69, 1.33 ± 0.34, and 0.42 ± 0.06%ID/g at 15, 30, and 60 min p.i., respectively). The early time liver uptake of ^{99m}Tc-PAboroxime (3.64 ± 0.92 and 3.39 ± 0.37% ID/g at 2 and 15 min p.i., respectively) was higher than that of ^{99m}Tc-Teboroxime (2.87 ± 0.67 and 2.22 ± 0.17%ID/g at 2 and 15 min p.i., respectively), but their liver uptake values were very close at >30 min p.i. In contrast, there was little liver radioactivity washout for ^{99m}Tc-ISboroxime (3.24 ± 0.55, 4.12 ± 1.30, 3.28 ± 0.78, and 3.13 ± 0.30%ID/g at 2, 15, 30, and 60 min p.i., respectively) over the 60 min study period. There was a significant radioactivity accumulation in blood vessels for ^{99m}Tc-PAboroxime (1.72 ± 0.48, 1.12 ± 0.34, 0.95 ± 0.35, and 0.21 ± 0.08%ID/g at 2, 15, 30, and 60 min p.i., respectively) and ^{99m}Tc-ISboroxime (1.92 ± 0.19, 1.01 ± 0.44, 0.92 ± 0.10, and 0.63 ± 0.23%ID/g at 2, 15, 30, and 60 min p.i., respectively). Similar blood vessel radioactivity accumulation was observed with ^{99m}Tc-Teboroxime, but not with cationic radiotracers, such as ^{99m}Tc-Sestamibi in the same animal model.[35−39]

SPECT Imaging in SD Rats. Figure 6A shows the coronal views of SPECT images from the SD rats administered with ^{99m}Tc-PAboroxime and ^{99m}Tc-ISboroxime, respectively. The right and left ventricular walls were clearly delineated. Despite their intense liver uptake (Figure 6B), high quality SPECT

DOI: 10.1021/bc500583k
Bioconjugate Chem. 2015, 26, 316−328

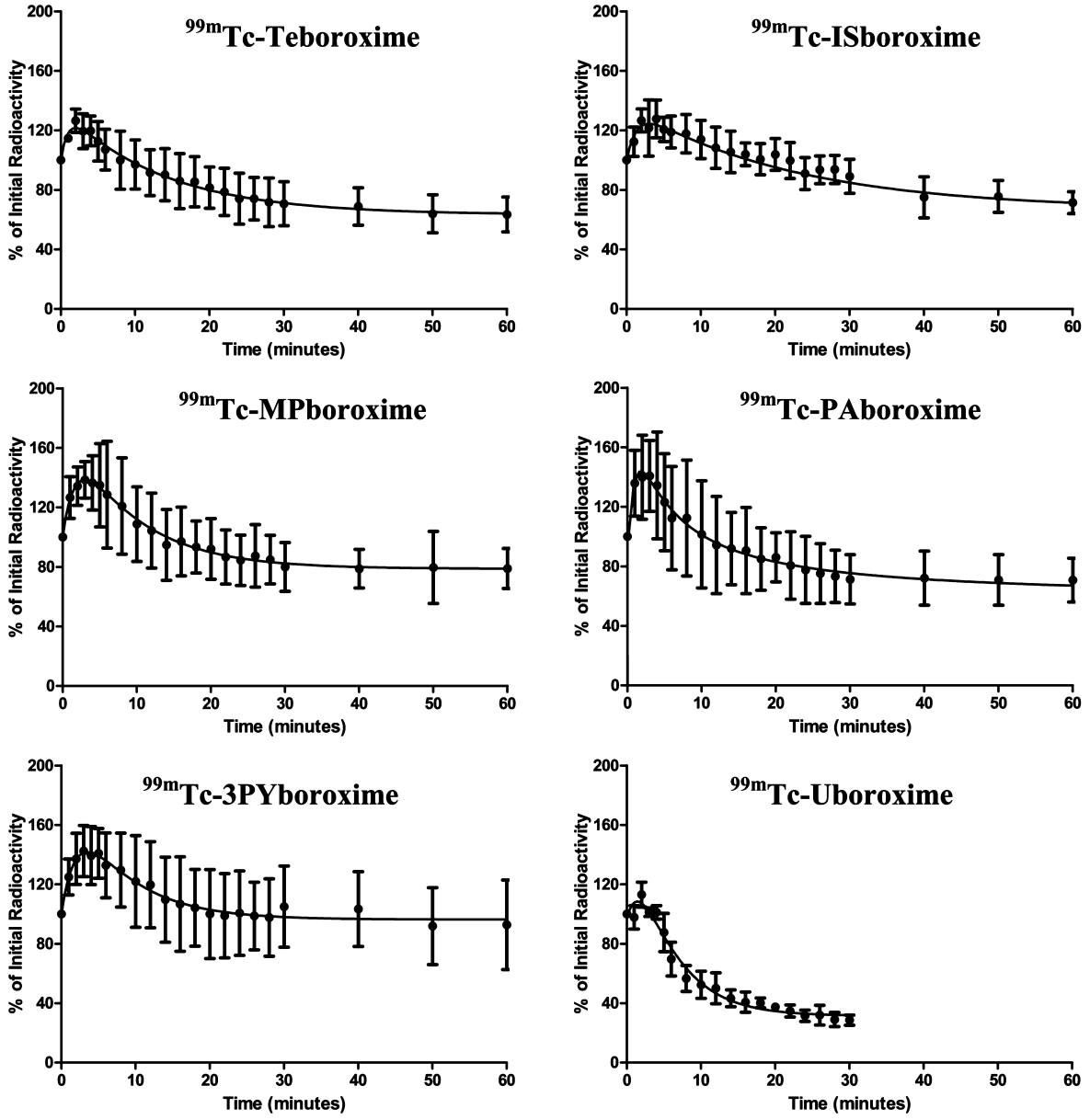

Figure 5. Imaging quantification data to compare liver clearance kinetics of ^{99m}Tc-Teboroxime, ^{99m}Tc-ISboroxime, ^{99m}Tc-MPboroxime, ^{99m}Tc-PAboroxime, ^{99m}Tc-PYboroxime, and ^{99m}Tc-Uboroxime. The quantification data were expressed as % of the initial liver uptake (0−1 min). The liver clearance curve was best fitted to a biexponential function using the individual animal time/activity data.

Table 2. Selected Biodistribution Data (%ID/g) and Heart/Organ Ratios for ^{99m}Tc-PAboroxime in SD Rats

organ	2 min (n = 7)	15 min (n = 6)	30 min (n = 4)	60 min (n = 4)
blood	0.49 ± 0.11	0.39 ± 0.10	0.41 ± 0.12	0.27 ± 0.08
brain	0.02 ± 0.01	0.02 ± 0.01	0.04 ± 0.04	0.01 ± 0.00
heart	3.05 ± 1.01	2.22 ± 0.17	1.59 ± 0.14	0.89 ± 0.19
intestines	1.03 ± 0.35	2.07 ± 0.86	3.71 ± 1.82	2.13 ± 0.87
kidneys	4.19 ± 1.02	2.02 ± 0.68	1.50 ± 0.38	0.76 ± 0.27
liver	3.64 ± 0.92	3.39 ± 0.37	2.80 ± 0.59	1.16 ± 0.53
lungs	1.80 ± 0.45	0.88 ± 0.18	0.68 ± 0.15	0.32 ± 0.08
muscle	0.21 ± 0.08	0.22 ± 0.07	0.33 ± 0.12	0.08 ± 0.02
spleen	2.19 ± 0.64	0.96 ± 0.21	0.56 ± 0.29	0.37 ± 0.13
vessels	1.72 ± 0.48	1.12 ± 0.34	0.95 ± 0.35	0.21 ± 0.08
heart/blood	5.72 ± 0.78	5.56 ± 0.65	4.00 ± 0.43	1.55 ± 0.36
heart/liver	0.85 ± 0.05	0.66 ± 0.16	0.56 ± 0.24	0.36 ± 0.12
heart/lung	1.69 ± 0.21	1.35 ± 0.12	1.78 ± 0.35	1.31 ± 0.21
heart/muscle	9.94 ± 1.65	6.12 ± 0.59	4.82 ± 1.19	5.25 ± 0.67

DOI: 10.1021/bc500583k
Bioconjugate Chem. 2015, 26, 316−328

Table 3. Selected Biodistribution Data (%ID/g) and Heart/Organ Ratios for ^{99m}Tc-ISboroxime in SD Rats

organ	2 min (n = 4)	15 min (n = 4)	30 min (n = 4)	60 min (n = 4)
blood	0.54 ± 0.20	0.35 ± 0.10	0.39 ± 0.08	0.26 ± 0.05
brain	0.10 ± 0.01	0.03 ± 0.01	0.03 ± 0.01	0.04 ± 0.01
heart	3.75 ± 0.68	1.68 ± 0.69	1.33 ± 0.34	0.42 ± 0.06
intestines	1.08 ± 0.16	1.19 ± 0.41	1.95 ± 0.66	4.13 ± 0.67
kidneys	3.85 ± 0.61	2.04 ± 0.72	1.91 ± 0.48	1.32 ± 0.14
liver	3.24 ± 0.55	4.12 ± 1.30	3.28 ± 0.78	3.13 ± 0.30
lungs	2.34 ± 0.93	1.27 ± 0.33	1.59 ± 0.76	0.88 ± 0.47
muscle	0.19 ± 0.04	0.34 ± 0.13	0.40 ± 0.18	0.28 ± 0.13
spleen	1.50 ± 0.53	1.81 ± 0.90	1.62 ± 0.53	1.17 ± 0.25
vessels	1.92 ± 0.19	1.01 ± 0.44	0.92 ± 0.10	0.63 ± 0.23
heart/blood	7.92 ± 2.85	4.65 ± 0.88	3.39 ± 0.24	3.48 ± 0.14
heart/liver	1.45 ± 0.53	0.40 ± 0.07	0.40 ± 0.02	0.42 ± 0.07
heart/lung	1.90 ± 0.65	1.31 ± 0.45	0.92 ± 0.20	0.89 ± 0.24
heart/muscle	20.16 ± 1.88	5.10 ± 1.58	3.39 ± 0.24	3.79 ± 1.31

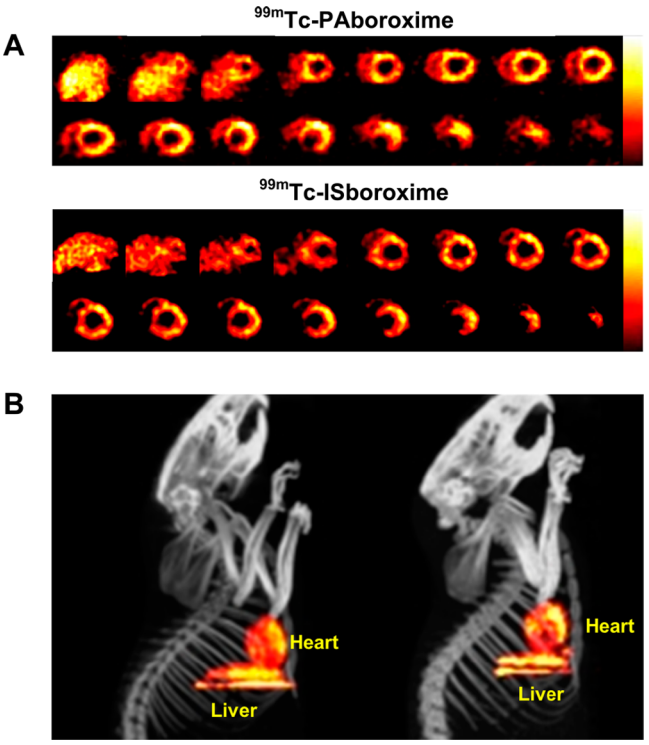

Figure 6. (A) Coronal views of SPECT images of the SD rats administered with 80−90 MBq of ^{99m}Tc-PAboroxime (upper panel) and ^{99m}Tc-ISboroxime (lower panel). Anesthesia was induced using an air flow rate of 350 mL/min and ∼3.0% isoflurane. SPECT images were obtained over first 5 min p.i. with the camera being focused in the heart region. Arrows indicate the presence of the liver radioactivity. Despite their intense liver uptake, high quality SPECT images could be acquired. (B) 3D views of SPECT/CT images of the SD rats administered with 80−90 MBq of ^{99m}Tc-Paboroxime (right panel) and ^{99m}Tc-ISboroxime (left panel) to illustrate radioactivity accumulation in the heart region.

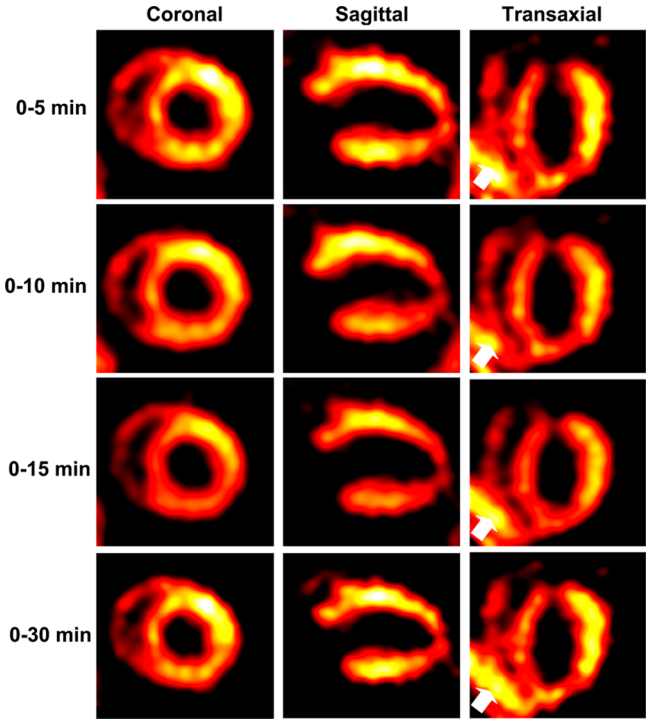

Figure 7. SPECT images of the SD rats administered with 80−90 MBq of ^{99m}Tc-PAboroxime. Anesthesia was induced using an air flow rate of 350 mL/min and ∼3.0% isoflurane. SPECT images were obtained with a camera being focused in the heart region. Arrows indicate the presence of liver radioactivity.

images were acquired. The best image acquisition window is 0−5 min for both ^{99m}Tc-PAboroxime and ^{99m}Tc-ISboroxime due to their high initial uptake (Table 1). Longer acquisition time did not improve the image quality due to its fast myocardial washout (Figure 4) and prolonged liver accumulation (Figure 6). In the transaxial SPECT images (Figure 7), the liver radioactivity overlapped significantly with that in the heart at the bottom of the right ventricle. This was particularly true in the SPECT images acquired during 0−30 min p.i. The interference from liver radioactivity in coronal and sagittal images was not significant over the 30 min study period. Therefore, it is possible to use both standard and specialized cardiac SPECT cameras for MPI studies using ^{99m}Tc-PAboroxime as the radiotracer.

SPECT/CT Imaging in Pigs. Figure 8A shows coronal views of SPECT images from the pigs administered with ^{99m}Tc-PAboroxime. The stressed heart had more activity accumulation, most likely due to higher regional blood flow. Figure 8B shows SPECT/CT images (coronal, sagittal, and transaxial) of the pigs administered with ^{99m}Tc-PAboroxime at rest (upper panel) and under stress (lower panel). Once again, the best image acquisition window is 0−5 min. However, high quality

DOI: 10.1021/bc500583k
Bioconjugate Chem. 2015, 26, 316−328

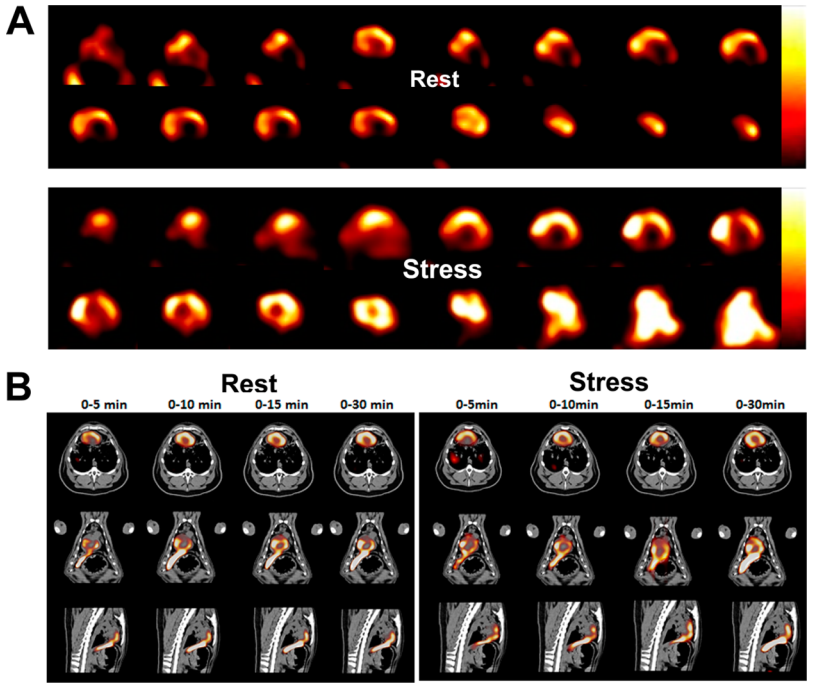

Figure 8. (A) Coronal views of SPECT images of the pig administered with ∼300 MBq of ^{99m}Tc-PAboroxime at rest (upper panel) and under stress (lower panel) to demonstrate its capability for early time dynamic imaging. SPECT images were obtained over the first 5 min p.i. using an E. cam SPECT (SIEMENS, Germany). (B) SPECT images of the pigs administered with ∼900 MBq of ^{99m}Tc-PAboroxime at rest (upper panel) and under stress (lower panel). SPECT images were obtained over the first 30 min postinjection to illustrate the optimal window for image data acquisition. Despite its intense liver activity accumulation, high quality SPECT images could be acquired over the first 30 min p.i. due to its longer myocardial retention as compared to that of ^{99m}Tc-PAboroxime.

SPECT/CT images of the pig heart could be readily acquired using the standard clinical SPECT cameras over the first 30 min p.i. These data were completely consistent with those obtained in the SD rats (Figure 6).

DISCUSSION

Successful development of efficient perfusion radiotracers remains the key for the future success of nuclear cardiology. In general, an ideal perfusion radiotracer should have a high heart uptake with stable myocardial retention, which would linearly track the regional blood flow over a wide range.[1−9,30−32] This linear relationship between radiotracer uptake and coronary blood flow rate up to ∼5 mL/min/g requires the radiotracer to have a high first-pass myocardial extraction, and is critically important for SPECT quantification, which has become possible with the development of new techniques for attenuation correction in SPECT/CT camera systems. The liver and lung uptake should be minimal so that diagnostically useful images of heart can be obtained within 30 min after administration of the radiotracer.

Over the past several years, we have been interested in cationic and neutral ^{99m}Tc complexes as SPECT radiotracers for heart imaging.[29,35−43] In this study, we evaluated five new ^{99m}Tc(III) complexes [^{99m}TcCl(CDO)(CDOH)$_2$B-R] (R = IS, MP, PA, PY, and 5U) for their potential as heart imaging agents. We found that the boronate capping groups have significant impact on their heart uptake, myocardial retention, and liver clearance. Among the radiotracers evaluated in planar imaging studies, ^{99m}Tc-PAboroxime shows longer myocardial retention time with the initial heart uptake (Table 1) comparable to that of ^{99m}Tc-Teboroxime.[29] This observation has been substantiated by biodistribution data (Table 2) and SPECT/CT imaging studies (Figure 7). The best image acquisition window is 0−5 min for ^{99m}Tc-PAboroxime and ^{99m}Tc-ISboroxime (Figure 6). However, high quality SPECT images were obtained during the first 30 min only with ^{99m}Tc-PAboroxime. ^{99m}Tc-PAboroxime also has advantages over ^{99m}Tc-Teboroxime and ^{99m}Tc-ISboroxime with respect to their lung uptake (Tables 2 and 3). The combination of high heart uptake and longer myocardial retention suggests that it is possible to image the heart with ^{99m}Tc-PAboroxime using both standard and specialized cardiac SPECT cameras. This statement is completely supported by the SPECT/CT data (Figure 8) obtained in normal pigs both at rest and under stress conditions.

A major shortcoming associated with ^{99m}Tc-PAboroxime is still its intense and prolonged liver uptake (Figure 6), which will interfere with the visualization of inferior wall of the heart using the standard clinical SPECT cameras (Figure 7). For the specialized cardiac SPECT cameras with cadmium−zinc−telluride detector,[19−26] however, it is possible to position the patient upright during image acquisition, which would definitely help minimize this interference because the liver tends to drop downward in this position, allowing better separation of the cardiac and hepatic radioactivity.

Minimizing photon scattering from the liver radioactivity remains a significant challenge in developing new SPECT and PET perfusion radiotracers for MPI. Over the past 30 years, many ether-containing ligands or chelators have been used to improve liver clearance kinetics of ^{99m}Tc radiotracers. This has been exemplified by successful development of ^{99m}Tc-Sestamibi and ^{99m}Tc-Tetrofosmin as radiotracers for SPECT MPI in clinics. More recent examples include ^{99m}TcN-DBODC5[44−46] and ^{99m}TcN-MPO.[38−43] It has been reported that high quality

DOI: 10.1021/bc500583k
Bioconjugate Chem. 2015, 26, 316−328

SPECT images were obtained as early as 10−15 min after injection due to their faster liver clearance than that of ^{99m}Tc-Sestamibi.[47,48] However, their heart uptake and first-pass extraction fraction also suffered significantly. It was reported that the first-pass extraction fractions of ^{99m}TcN-DBODC5 and ^{99m}TcN-MPO are most likely between those of ^{99m}Tc-Sestamibi and ^{99m}Tc-Tetrofosmin.[38,43] In this study, we show that the boronate capping groups can be used to increase the myocardial retention time of ^{99m}Tc radiotracers. However, it was more difficult to minimize the liver radioactivity without changing the heart uptake and myocardial retention time of the radiotracer.

One might ask if it is really possible to decrease the liver radioactivity accumulation while maintaining its high heart uptake. The answer to this question lies in localization mechanism, overall molecular charge, lipophilicity, and molecular shape of the radiotracer. Myocytes and hepatocytes have the highest mitochondrial density. The radiotracers currently available or under clinical evaluation are almost exclusively mitochondrion-targeted either by binding to enzymes embedded in the mitochondrial membrane or by localizing inside mitochondria due to the negative mitochondrial potential. Since it is easy for small organic molecules to penetrate the cellular and mitochondrial membranes, the neutral radiotracers, such as ^{18}F-BMS747158-02,[49−53] tend to have a high first-pass extraction fraction. High liver uptake was also seen in the whole-body images of human subjects administered with ^{18}F-BMS747158-02.[54] ^{99m}TcN-NOET is a neutral radiotracer with a high first-pass extraction fraction,[55−58] but its high uptake in the liver and lungs imposes a significant hurdle for its widespread clinical acceptance. For cationic radiotracers (e.g., ^{99m}Tc-Sestamibi and ^{99m}Tc-Tetrofosmin), the penetration of mitochondrial membrane becomes more difficult because of the extra molecular charge, leading to their relatively low first-pass extraction. Thus, it is not an easy task to decrease the liver radioactivity and maintain high heart uptake at the same time for the mitochondrion-targeted ^{99m}Tc-radiotracers because liver is a mitochondrion-rich organ. There is always a subtle balance between the heart uptake and liver radioactivity.

The choice of a radiotracer will largely depend on the purpose of MPI studies. If the MPI study is simply to determine whether the patient has ischemia or myocardial infarction, cationic radiotracers (such as ^{99m}Tc-Sestamibi, ^{99m}Tc-Tetrofosmin, or ^{99m}TcN-MPO) would be sufficient because there is no need for a linear relationship between the radiotracer heart uptake and blood flow rates. If the objective of MPI study is to define the extent and severity of disease, assess myocardial viability, and predict future heart events in CAD patents, then it will require precise measurement of the regional blood flow and the direct linear relationship between the radiotracer heart uptake and blood flow rates. In this situation, ^{99m}Tc-Teboroxime and ^{99m}Tc-PAboroxime would be the radiotracers of choice due to their high initial heart uptake. The first-pass myocardial extraction fraction of ^{99m}Tc-PAboroxime has not been determined. However, it is reasonable to believe that it might be very close to that of ^{99m}Tc-Teboroxime on the basis of their 2 min biodistribution data (Table 2) and the results from planar image studies (Table 1).

The heart uptake mechanism of ^{99m}Tc(III) complexes [^{99m}TcCl(CDO)(CDOH)$_2$B-R] (R = IS, MP, PA, PY, and 5U) is not known. It also remains unknown if they are able to enter myocytes or attach to phospholipid layers of the cellular and/or mitochondrial membranes. It has been suggested that [^{99m}Tc(H$_2$O)(CDO)(CDOH)$_2$BMe]$^+$ is responsible for the high heart uptake of ^{99m}Tc-Teboroxime.[33] This assumption seems to be supported by the very low heart uptake of ^{99m}Tc-MPboroxime with an extra positive charge on the pyridinium moiety (Figure 1). The extra charge makes it more difficult for ^{99m}Tc-MPboroxime to cross both the cellular and mitochondrial membranes. However, this assumption is not supported by low heart uptake and fast myocardial washout of ^{99m}Tc-5Uboroxime that shares the same molecular charge with ^{99m}Tc-PAboroxime. Therefore, there must be an alternative mechanism for the myocardial localization of ^{99m}Tc(III) complexes [^{99m}TcCl(CDO)(CDOH)$_2$B-R].

CONCLUSIONS

In this study, we found that the boronate-capping groups have significant impact on the heart uptake, myocardial retention, and liver clearance kinetics of ^{99m}Tc(III) radiotracers. ^{99m}Tc-PAboroxime has initial heart uptake comparable to that of ^{99m}Tc-Teboroxime with a longer myocardial retention, which makes it possible to image the heart with both standard and specialized cardiac SPECT cameras using ^{99m}Tc-PAboroxime as the radiotracer.

EXPERIMENTAL METHODS

Materials. Chemicals (citric acid, γ-cyclodextrin, cyclohexanedione dioxime (CDOH), diethylenetriaminepentaacetic acid (DTPA), isoxazole-4-boronic acid, methylboronic acid, 1*H*-pyrazol-3-ylboronic acid, 3-pyridineboronic acid, *N*-methylpyridinium-4-boronic acid iodide, sodium chloride, stannous chloride dihydrate, and uracil-5-boronic acid) were purchased from Sigma/Aldrich (St. Louis, MO), and were used without purification. Na^{99m}TcO$_4$ were obtained from Cardinal Health-Care (Chicago, IL).

Radio-HPLC Method. The radio-HPLC method for analysis of new ^{99m}Tc(III) complexes [^{99m}TcCl(CDO)-(CDOH)$_2$B-R] (R = IS, MP, PA, PY, and 5U) used an Agilent HP-1100 HPLC system (Agilent Technologies, Santa Clara, CA) equipped with a β-ram IN/US detector (Tampa, FL) and Zorbax C$_8$ column (4.6 mm × 250 mm, 300 Å pore size; Agilent Technologies, Santa Clara, CA). The flow rate was 1 mL/min. The mobile phase was isocratic with 30% solvent A (10 mM NH$_4$OAc buffer, pH = 6.8) and 70% solvent B (methanol) between 0 and 5 min, followed by a gradient from 70% solvent B at 5 min to 90% solvent B at 15 min, and isocratic mobile phase with 10% solvent A and 90% solvent B. The instant thin layer chromatography (ITLC) used Gelman Sciences silica-gel strips and a 1:1 mixture of acetone and saline as the mobile phase. ^{99m}Tc(III) complexes and ^{99m}TcO$_4^-$ migrated to the solvent front while [^{99m}Tc]colloid stayed at the origin. [^{99m}Tc]colloid was determined as the percentage of radioactivity at the origin over the total radioactivity on each strip.

Preparation of [^{99m}TcCl(CDO)(CDOH)$_2$B-R] (R = IS, MP, PA, PY, and 5U). All new ^{99m}Tc(III) radiotracers were prepared using the kit formulation.[29,34] Each lyophilized vial contains 2 mg of CDOH$_2$, 2 mg of boronic acid derivative, 50 μg of SnCl$_2$·2H$_2$O, 9 mg of citric acid, 2 mg of DTPA, 20 mg of NaCl, and 20 mg of γ-cyclodextrin. To a lyophilized vial was added 1.0 mL ^{99m}TcO$_4^-$ solution (370−1110 MBq). The vial was then heated at 100 °C for 10−15 min. After reaction, a sample of the resulting solution was diluted with saline

DOI: 10.1021/bc500583k
Bioconjugate Chem. 2015, 26, 316−328

containing ~20% propylene glycol to 3.7 MBq/mL. The diluted solution was analyzed by HPLC and ITLC. Propylene glycol was used to minimize adsorption of highly lipophilic ^{99m}Tc radiotracers. The radiochemical purity (RCP) was 90−98% with a minimal amount of [^{99m}Tc]colloid (<0.5%). Their solution stability was monitored by radio-HPLC at 0, 2, 4, and 6 h postlabeling.

Doses Preparation. Doses for biodistribution were prepared by dissolving radiotracer kit solution to ~1.1 MBq/mL with saline containing 20% propylene glycol. The injection volume was 0.1 mL for each animal for biodistribution studies. Doses for imaging studies were made by dissolving the ^{99m}Tc radiotracer solution to ~370 MBq/mL with saline containing 20% propylene glycol. All dose solutions were filtered with a 0.20 μm filter unit to eliminate foreign particles before being injected into animals. The injection volume was ~0.1 mL per animal for biodistribution and 0.2−0.5 mL per animal for imaging studies.

Animal Preparation. Animal studies were conducted in compliance with the NIH animal experiment guidelines (*Principles of Laboratory Animal Care*, NIH Publication No. 86−23, revised 1985). The protocols for biodistribution and imaging studies were approved by the Purdue University Animal Care and Use Committee (PACUC). The SD rats (200−250 g) were purchased from Harlan (Indianapolis, IN), and were acclimated for more than 24 h. Animals were anesthetized with intramuscular injection of a mixture of ketamine (80 mg/kg) and xylazine (19 mg/kg) before being used for biodistribution and planar imaging studies.

Biodistribution. The SD rats (8−12 females and 8−12 males) were randomly divided into four groups. Each animal was administered with 100−111 KBq of ^{99m}Tc radiotracer via the tail vein. Animals (4−6) were sacrificed by sodium pentobarbital overdose (100−200 mg/kg) at 2, 15, 30, and 60 min p.i. Blood was withdrawn from the heart. Organs of interest (heart, brain, lungs, liver, spleen, kidneys, muscle, and intestines) were excised, rinsed with saline, dried with absorbent tissues, weighed, and counted on a PerkinElmer Wizard-1480 γ-counter (Shelton, CT). Six extra doses were also weighed and counted before and after organ tissue samples. Organ uptake was calculated and reported as the percentage of injected dose (%ID/g) or the percentage of injected dose per gram of wet mass (%ID/g).

Dynamic Planar Imaging in SD Rats. Dynamic planar imaging studies were performed in SD rats (3 females and 3 males). Each animal was administered with ^{99m}Tc radiotracer (90−100 MBq) in 0.2 mL of saline via the tail vein. The animal was placed prone on a single head mini γ-camera (Diagnostic Services Inc., NJ). A standard radiation source with a known amount of radioactivity was placed beside the animal. The 1 min static images were acquired during the first 5 min p.i., followed by the 2 min static images at 6−30, 40, 50, and 60 min p.i. The imaging data were stored digitally in a 128 × 128 matrix. After imaging, animals were returned to a lead-shielded cage to recover. The images were analyzed by drawing regions of the organ of interest (heart and liver) and radiation source. The results were corrected for background. The results were expressed as the percentage of injected dose (%ID/g) in the heart, or a percentage of the initial radioactivity accumulation in the liver. The exponential fit of heart retention and liver clearance was determined using GraphPad Prim 5.0 (GraphPad Software, Inc., San Diego, CA).

SPECT Imaging in SD Rats. SPECT images of SD rats (n = 2) were obtained with ^{99m}Tc-ISboroxime and ^{99m}Tc-PAboroxime using the u-SPECT-II/CT scanner (Milabs, Utrecht, The Netherlands) equipped with a 1.0 mm multipinhole collimator. The animal was placed into a shielded chamber connected to an isoflurane anesthesia unit (Univentor, Zejtun, Malta). Anesthesia was induced using an air flow rate of 350 mL/min and ~3.0% isoflurane, and maintained using an air flow of ~250 mL/min with ~2.5% isoflurane during preparation and image data acquisition (6 frames: 75 projections over 5 min per frame). The animal was administered with the ^{99m}Tc radiotracer (~180 MBq) in 0.5 mL saline containing ~20% propylene glycol through a catheter, followed with 0.5 mL saline solution flash. Rectangular scan in regions of interest (ROIs) from SPECT and CT were selected on the basis of the orthogonal X-ray images provided by the CT. After SPECT acquisition, the animal was allowed to recover in a shielded cage.

Image Reconstruction and Data Processing. SPECT reconstruction was performed using a POSEM (pixelated ordered subsets by expectation maximization) algorithm with 6 iterations and 16 subsets. CT data were reconstructed using a cone-beam filtered back-projection algorithm (NRecon v 1.6.3, Skyscan). After reconstruction, the SPECT and CT data were automatically co-registered according to the movement of the robotic stage, and re-sampled to equivalent voxel sizes. Co-registered images were further rendered and visualized using the PMOD software (PMOD Technologies, Zurich, Switzerland). A 3D-Guassian filter (1.2 mm fwhm) was applied to smooth noise, and the LUTs (look up tables) were adjusted for good visual contrast. The images were visualized as both orthogonal slices and maximum intensity projections.

SPECT/CT Imaging in Pigs. SPECT/CT studies were performed in normal pigs (n = 2, 23−26 kg, 1 female and 1 male). The protocol for animal studies in pigs was approved by the Fu Wai Hospital Animal Care and Use Committee (Beijing, China). The rest and stress SPECT myocardial perfusion images were acquired according to one-day protocol. The animals were anesthetized with intravascular injection of 3% pentobarbital sodium (30 mg/kg). Additional sodium pentobarbital were used via i.v. injection to maintain anesthesia, when needed. During imaging, animals were maintained with mechanical ventilation and monitored with electrocardiogram (ECG). CT images were acquired using the CT component of a PET-CT camera (Biograph64-Truepoint PET-CT, SIEMENS, Germany). The animal was kept in the same position, and was then injected with ^{99m}Tc-Paboroxime (~300 MBq), followed with 2 mL saline solution to flush the tube. Dynamic images (6 frames: 5 min per frame) were immediately obtained using a SPECT camera (E. cam SPECT, SIEMENS, Germany). When the rest of the image acquisition was completed, the adenosine disodium triphosphate (ATP, Henan, China) was injected through the vein in left ear edge in the speed of 0.16 mg/min/kg with an injection pump. After 2.5 min, the animal was administered with ^{99m}Tc-Paboroxime (~900 MBq) in 5 mL saline through the femoral vein, followed with 2 mL saline solution to flush the tube. The dynamic SPECT images (6 frames: 5 min per frame) were obtained under stress conditions. The ATP injection was stopped in 8 min. After image acquisition, the SPECT and CT data were processed with Amide.exe 1.0.4 (Sourceforge, United States) and ImageJ 1.49 (the National Institutes of Health, United States) and co-registered manually.

DOI: 10.1021/bc500583k
Bioconjugate Chem. 2015, 26, 316−328

Data and Statistical Analysis. Biodistribution data, T/B ratios, and imaging quantification data were reported as an average ± standard deviation based on the results from four to six SD rats at each time point. Comparison between two radiotracers was made using a one-way ANOVA test. The level of significance was set at $p < 0.05$.

■ ASSOCIATED CONTENT

Supporting Information

SPECT images of the SD rats administered with 80−90 MBq of ^{99m}Tc-ISboroximine. This material is available free of charge via the Internet at http://pubs.acs.org.

■ AUTHOR INFORMATION

Corresponding Authors

*(W.F.) E-mail: nuclearfw@126.com. Phone: 86-10-88398482. Fax: 86-10-88393012.

*(S.L.) E-mail: liu100@purdue.edu. Phone: 765-494-0236. Fax: 765-496-1377.

Notes

The authors declare no competing financial interest.

■ ACKNOWLEDGMENTS

This work was supported, in part, by Purdue University, the Indiana Clinical and Translational Sciences Institute funded in part by grant Number TR000006 (Clinical and Translational Award) from the National Institutes of Health, the National Center for advancing Translational Science, R21 EB017237-01 (S.L.) from the National Institute of Biomedical Imaging and Bioengineering (NIBIB), and grant 81401446 from the National Nature Science Foundation of China (Y.Z.).

■ ABBREVIATIONS

BATO, boronic acid adducts of technetium dioximes; CT, computed tomography; DTPA, diethylenetriaminepentaacetic acid (or pentetic acid); FDA, Food and Drug Administration; SPECT, single photon-emission computed tomography; ^{99m}TcN-DBODC5, $[^{99m}TcN(DBODC)(PNP5)]^+$ (PNP5 = *N*-ethoxyethyl-*N*,*N*-bis[2-(bis(3-methoxypropyl)phosphino)-ethyl]amine and DBODC = *N*,*N*-bis(ethoxyethyl)-dithiocarbamate); ^{99m}TcN-MPO, $[^{99m}TcN(mpo)(PNP5)]^+$ (mpo = 2-mercaptopyridine oxide); ^{99m}TcN-NOET, $^{99m}TcN(NOET)_2$ (NOET = *N*-ethoxy-*N*-ethyldithiocarbamato); ^{99m}Tc-Sestamibi, $[^{99m}Tc(MIBI)_6]^+$ (MIBI = 2-methoxy-2-methylpropylisonitrile); ^{99m}Tc-Tetrofosmin, $[^{99m}TcO_2(tetrofosmin)_2]^+$ (tetrofosmin = 1,2-bis[bis(2-ethoxyethyl)phosphino]ethane); ^{99m}Tc-Teboroxime, $[^{99m}TcCl(CDO)(CDOH)_2BMe]$ (CDOH = cyclohexanedione dioxime); ^{99m}Tc-ISboroxime, $[^{99m}TcCl(CDO)(CDOH)_2B(isoxazol\text{-}4\text{-}yl)]$; ^{99m}Tc-MPboroxime, $[^{99m}TcCl(CDO)(CDOH)_2B(N\text{-}methylpyridinium\text{-}4\text{-}yl)]$; ^{99m}Tc-PAboroxime, $[^{99m}TcCl(CDO)(CDOH)_2B(1H\text{-}pyrazol\text{-}3\text{-}yl)]$; ^{99m}Tc-PYTeboroxime, $[^{99m}TcCl(CDO)(CDOH)_2B(pyridin\text{-}3\text{-}yl)]$; ^{99m}Tc-5Uboroxime, $[^{99m}TcCl(CDO)(CDOH)_2B(uracil\text{-}5\text{-}yl)]$

■ REFERENCES

(1) Nunn, A. D. (1990) Radiopharmaceuticals for imaging myocardial perfusion. *Semin. Nucl. Med. 20*, 111−118.

(2) Kailasnath, P., and Sinusas, A. J. (2001) Comparison of Tl-201 with Tc-99m-labeled myocardial perfusion agents: technical, physiological, and clinic issues. *J. Nucl. Cardiol. 8*, 482−498.

(3) Jain, D. (1999) Technetium-99m labeled myocardial perfusion imaging agents. *Semin. Nucl. Med. 29*, 221−236.

(4) Acampa, W., Di Benedetto, C., and Cuocolo, A. (2000) An overview of radiotracers in nuclear cardiology. *J. Nucl. Cardiol. 7*, 701−707.

(5) Banerjee, S., Pillai, M. R., and Ramamoorthy, N. (2001) Evolution of Tc-99m in diagnostic radiopharmaceuticals. *Semin. Nucl. Med. 31*, 260−277.

(6) Baggish, A. L., and Boucher, C. A. (2008) Radiopharmaceutical agents for myocardial perfusion imaging. *Circulation 118*, 1668−1674.

(7) Llaurado, J. G. (2001) The quest for the perfect myocardial perfusion indicator···still a long way to go. *J. Nucl. Med. 42*, 282−284.

(8) Henneman, M. M., Schuijf, J. D., van der Wall, E. E., and Bax, J. J. (2006) Non-invasive anatomical and functional imaging for the detection of coronary artery disease. *Br. Med. Bull. 79−80*, 187−202.

(9) Stirrup, J., Wechalekar, K., Maenhout, A., and Anagnastopoulos, C. (2009) Cardiac radionuclide imaging in stable coronary artery disease and acute coronary syndromes. *Br. Med. Bull. 89*, 63−78.

(10) Rumsey, W. L., Rosenspire, K. C., and Nunn, A. D. (1992) Myocardial extraction of teboroxime: effects of teboroxime interaction with blood. *J. Nucl. Med. 33*, 94−101.

(11) Marshall, R. C., Leidholdt, E. M., Jr., Zhang, D. Y., and Barnett, C. A. (1991) The effect of flow on technetium-99m-teboroxime (SQ30217) and thallium-201 extraction and retention in rabbit heart. *J. Nucl. Med. 32*, 1979−1988.

(12) Leppo, J. A., and Meerdink, D. J. (1990) Comparative myocardial extraction of two technetium-labeled BATO derivatives (SQ30217, SQ32014) and thallium. *J. Nucl. Med. 31*, 67−74.

(13) Williams, K. A., Taillon, L. A., Draho, J. M., and Foisy, M. F. (1993) First-pass radionuclide angiographic studies of left ventricular function with technetium-99m-teboroxime, technetium-99m-sestamibi and technetium-99m-DTPA. *J. Nucl. Med. 34*, 394−399.

(14) Johnson, L. L. (1994) Myocardial perfusion imaging with technetium-99m-teboroxime. *J. Nucl. Med. 35*, 689−692.

(15) Seldin, D. W., Johnson, L. L., Blood, D. K., Muschel, M. J., Smith, K. F., and Wall, R. M. (1989) Myocardial perfusion imaging with technetium-99m SQ30217: comparison with thallium-201 and coronary anatomy. *J. Nucl. Med. 30*, 312−319.

(16) McSherry, B. A. (1991) Technetium-99m-Teboroxime: a new agent for myocardial perfusion imaging. *J. Nucl. Med. Technol. 19*, 22−26.

(17) Iskandrian, A. S., Heo, J., Nguyen, T., and Mercuro, J. (1991) Myocardial imaging with Tc-99m teboroxime: technique and initial results. *Am. Heart J. 121*, 889−894.

(18) Fleming, R. M., Kirkeeide, R. L., Taegtmeyer, H., Adyanthaya, A., Cassidy, D. B., and Goldstein, R. A. (1991) Comparison of technetium-99m teboroxime tomography with automated quantitative coronary arteriography and thallium-201 tomographic imaging. *J. Am. Coll. Cardiol. 17*, 1297−1302.

(19) Esteves, F. P., Raggi, P., Folks, R. D., Keidar, Z., Askew, J. W., Rispler, S., O'Connor, M. K., Verdes, L., and Garcia, E. V. (2009) Novel solid-state-detector dedicated cardiac camera for fast myocardial perfusion imaging: multicenter comparison with standard dual detector cameras. *J. Nucl. Cardiol. 16*, 927−934.

(20) Buechel, R. R., Pazhenkottil, A. P., Herzog, B. A., Husmann, L., Nkoulou, R. N., Burger, I. A., Valenta, I., Wyss, C. A., Ghadri, J. R., and Kaufmann, P. A. (2010) Real-time breath-hold triggering of myocardial perfusion imaging with a novel cadmium-zinc-telluride detector gamma camera. *Eur. J. Nucl. Med. Mol. Imaging 37*, 1903−1908.

(21) Duvall, W. L., Croft, L. B., Godiwala, T., Ginsberg, E., George, T., and Henzlova, M. J. (2010) Reduced isotope dose with rapid SPECT MPI imaging: initial experience with a CZT SPECT camera. *J. Nucl. Cardiol. 17*, 1009−1014.

(22) Pazhenkottil, A. P., Buechel, R. R., Herzog, B. A., Nkoulou, R. N., Valenta, I., Fehlmann, U., Ghadri, J. R., Wolfrum, M., Husmann, L., and Kaufmann, P. A. (2010) Ultrafast assessment of left ventricular dyssynchrony from nuclear myocardial perfusion imaging on a new

DOI: 10.1021/bc500583k
Bioconjugate Chem. 2015, 26, 316−328

high-speed gamma camera. *Eur. J. Nucl. Med. Mol. Imaging 37*, 2086−2092.
(23) Schillaci, O., and Danieli, R. (2010) Dedicated cardiac cameras: a new option for nuclear myocardial perfusion imaging. *Eur. J. Nucl. Med. Mol. Imaging 37*, 1706−1709.
(24) Tsai, W. K., Holohan, K. M., and Williams, K. A. (2010) Myocardial perfusion imaging from echocardiography to SPECT, PET, CT, and MRI—recent advances and applications. *US Cardiology 7*, 12−16.
(25) Gaemperli, O., and Kaufmann, P. A. (2011) Lower dose and shorter acquisition: pushing the boundaries of myocardial perfusion SPECT. *J. Nucl. Cardiol. 18*, 830−832.
(26) Fiechter, M., Ghadri, J. R., Kuest, S. M., Pazhenkottil, A. P., Wolfrum, M., Nkoulou, R. N., Goetti, R., Gaemperli, O., and Kaufmann, P. A. (2011) Nuclear myocardial perfusion imaging with a novel cadmium-zinc-telluride detector SPECT/CT device: first validation versus invasive coronary angiography. *Eur. J. Nucl. Med. Mol. Imaging 38*, 2025−2030.
(27) Bailey, D. L., and Willowson, K. P. (2013) An evidence-based review of quantitative SPECT imaging and potential clinical applications. *J. Nucl. Med. 54*, 83−89.
(28) Salerno, M., and Beller, G. A. (2009) Noninvasive assessment of myocardial perfusion. *Circ. Cardiovasc. Imaging 2*, 412−424.
(29) Zheng, Y., Ji, S., Tomaselli, E., Ernest, C., Freiji, T., and Liu, S. (2014) Effect of co-ligands on chemical and biological properties of ^{99m}Tc(III) complexes [^{99m}Tc(L)(CDO)(CDOH)$_2$BMe] (L = Cl, F, SCN and N_3; $CDOH_2$ = cyclohexanedione dioxime). *Nucl. Med. Biol. 2*, 412−424.
(30) Beller, G. A., and Zaret, B. L. (2001) Contributions of nuclear cardiology to diagnosis and prognosis of patients with coronary artery disease. *Circulation 101*, 1465−1478.
(31) Parker, J. A. (2001) Cardiac nuclear medicine in monitoring patients with coronary heart disease. *Semin. Nucl. Med. 31*, 223−237.
(32) Kapur, A., Latus, K. A., Davies, G., Dhawan, R. T., Eastick, S., Jarritt, P. H., Roussakis, G., Young, M. C., Anagnostopoulos, C., Bomanji, J., Costa, D. C., Pennell, D. J., Prvuloich, E. M., Ell, P. J., and Underwood, S. R. (2002) A comparison of three radionuclide myocardial perfusion tracers in clinical practice: the ROBUST study. *Eur. J. Nucl. Med. Mol. Imaging 29*, 1608−1616.
(33) Treher, E. N., Francesconi, L. C., Gougoutas, J. Z., Malley, M. F., and Nunn, A. D. (1989) Monocapped Tris(dioxime) complexes of technetium(III): synthesis and structural characterization of TcX-(dioxime)$_3$B-R (X = Cl, Br; dioxime = dimethylglyoxime, cyclohexanedione dioxime; R = CH_3, C_4H_9). *Inorg. Chem. 28*, 3411−3416.
(34) Jurisson, S. S., Hirth, W., Linder, K. E., Di Rocco, R. J., Narra, R. K., and Nowotnik, D. P. (1991) Chloro→hydroxy substitution on technetium BATO [TcCl(dioxime)$_3$BR] complexes. *Int. J. Rad. Appl. Instrum. B 18*, 735−744.
(35) Liu, S., He, Z. J., Hsieh, W. Y., and Kim, Y. S. (2006) Evaluation of novel cationic ^{99m}Tc-nitrido complexes radiopharmaceuticals for heart imaging: improving liver clearance with crown ether groups. *Nucl. Med. Biol. 33*, 419−432.
(36) He, Z. J., Hsieh, W. Y., Kim, Y. S., and Liu, S. (2006) Evaluation of novel cationic ^{99m}Tc(I)-tricarbonyl complexes as potential radiotracers for myocardial perfusion imaging. *Nucl. Med. Biol. 33*, 1045−1053.
(37) Liu, S., He, Z. J., Hsieh, W. Y., and Kim, Y. S. (2007) Impact of bidentate chelators on lipophilicity, stability and biodistribution characteristics of cationic ^{99m}Tc-nitrido complexes. *Bioconjugate Chem. 18*, 929−936.
(38) Kim, Y. S., Wang, J., Broisat, A., Glover, D. K., and Liu, S. (2008) ^{99m}Tc-N-MPO: novel cationic ^{99m}Tc radiotracer for myocardial perfusion imaging. *J. Nucl. Cardiol. 15*, 535−546.
(39) Kim, Y. S., Shi, J., Zhai, S., Hou, G., and Liu, S. (2009) Mechanism for myocardial localization and rapid liver clearance of ^{99m}Tc-N-MPO: a new perfusion radiotracer for heart imaging. *J. Nucl. Cardiol. 16*, 571−579.
(40) Liu, S. (2007) Ether and crown ether-containing cationic ^{99m}Tc complexes useful as radiopharmaceuticals for heart imaging. *Dalton Trans. 28*, 1183−1193.
(41) Kim, Y. S., Wang, F., and Liu, S. (2010) Minimizing liver uptake of cationic ^{99m}Tc radiotracers with ether and crown ether functional groups. *World J. Hematol. 2*, 21−31.
(42) Bu, L., Li, R., Jin, Z., Wen, X., Liu, S., Yang, B., Shen, B., and Chen, X. (2011) Evaluation of ^{99m}TcN-MPO as a new myocardial perfusion imaging agent in normal dogs and in an acute myocardial infarction canine model: comparison with ^{99m}Tc-sestamibi. *Mol. Imaging Biol. 13*, 121−127.
(43) Zheng, Y., Ji, S., Tomaselli, E., and Liu, S. (2014) Formulation development for preparation of ^{99m}TcN-MPO: a cationic SPECT radiotracer for myocardial perfusion imaging. *J. Labeled Compd. Radiopharm. 57*, 584−592.
(44) Boschi, A., Uccelli, L., Bolzati, C., Duatti, A., Sabba, N., Moretti, E., Di Domenico, G., Zavattini, G., Refosco, F., and Giganti, M. (2003) Synthesis and biologic evaluation of monocationic asymmetrical ^{99m}Tc-nitride heterocomplexes showing high heart uptake and improved imaging properties. *J. Nucl. Med. 44*, 806−814.
(45) Hatada, K., Riou, L. M., Ruiz, M., Yamamichi, Y., Duatti, A., Lima, R. L., Goode, A. R., Watson, D. D., Beller, G. A., and Glover, D. K. (2004) ^{99m}Tc-N-DBODC5, a new myocardial perfusion imaging agent with rapid liver clearance: comparison with ^{99m}Tc-Sestamibi and ^{99m}Tc-Tetrofosmin in rats. *J. Nucl. Med. 45*, 2095−2101.
(46) Hatada, K., Ruiz, M., Riou, L. M., Lima, R. L., Goode, A. R., Watson, D. D., Beller, G. A., and Glover, D. K. (2006) Organ biodistribution and myocardial uptake, washout, and redistribution kinetics of Tc-99m N-DBODC5 when injected during vasodilator stress in canine models of coronary stenoses. *J. Nucl. Cardiol. 13*, 779−790.
(47) Cittanti, C., Uccelli, L., Pasquali, M., Boschi, A., Flammia, C., Bagatin, E., Casali, M., Stabin, M. G., Feggi, L., Giganti, M., and Duatti, A. (2008) Whole-body biodistribution and radiation dosimetry of the new cardiac tracer ^{99m}Tc-N-DBODC. *J. Nucl. Med. 49*, 1299−1304.
(48) Gao, S., Zhao, G., Wen, Q., Bai, L., Chen, B., Ji, T., Ji, B., and Ma, Q. (2014) Pharmacokinetics and biodistribution of ^{99m}TcN-MPO in healthy human volunteers. *Clin. Nucl. Med. 39*, e14−e19.
(49) Yu, M., Guaraldi, M. T., Mistry, M., Kagan, M., McDonald, J. L., Drew, K., Yu, M., Guaraldi, M. T., Mistry, M., Kagan, M., McDonald, J. L., Drew, K., Radeke, H., Azure, M., Purohit, A., Casebier, D. S., and Robinson, S. P. (2007) BMS-747158−02: a novel PET myocardial perfusion imaging agent. *J. Nucl. Cardiol. 14*, 789−798.
(50) Yalamanchili, P., Wexler, E., and Hayes, M. (2007) Mechanism of uptake and retention of ^{18}F BMS-747158−02 in cardiomyocytes: a novel PET myocardial imaging agent. *J. Nucl. Cardiol. 14*, 782−788.
(51) Sherif, H. M., Saraste, A., Weidl, E., Weber, A. W., Higuchi, T., Reder, S., Poethko, T., Henriksen, G., Casebier, D., Robinson, S., Wester, H. J., Nekolla, S. G., and Schwaiger, M. (2009) Evaluation of a novel ^{18}F-Labeled positron-emission tomography perfusion tracer for the assessment of myocardial infarct size in rats. *Circ. Cardiovasc. Imaging 2*, 77−84.
(52) Nekolla, S. G., Reder, S., Saraste, A., Higuchi, T., Dzewas, G., Preissel, A., Huisman, M., Poethko, T., Schuster, T., Yu, M., Robinson, S., Casebier, D., Henke, J., Wester, H. J., and Schwaiger, M. (2009) Evaluation of the novel myocardial perfusion positron emission tomography tracer ^{18}F-BMS-747158−02: Comparison to ^{13}N-ammonia and validation with microspheres in a pig model. *Circulation 119*, 2333−2342.
(53) Yu, M., Guaraldi, M. T., Bozek, J., Kagan, M., Azure, M., Radeke, H., Cdebaca, M., and Robinson, S. P. (2009) Effects of food intake and anesthetic on cardiac imaging and uptake of BMS747158−02 in comparison with FDG. *J. Nucl. Cardiol 16*, 763−768.
(54) Maddahi, J., Czernin, J., Lazewatsky, J., Huang, S. C., Dahlbom, M., Schelbert, H., Sparks, R., Ehlgen, A., Crane, P., Zhu, Q., Devine, M., and Phelps, M. (2011) Phase I, first-in-human study of BMS747158, a novel ^{18}F-labeled tracer for myocardial perfusion PET: Dosimetry, biodistribution, safety, and imaging characteristics after a single injection at rest. *J. Nucl. Med. 52*, 1490−1498.

DOI: 10.1021/bc500583k
Bioconjugate Chem. 2015, 26, 316−328

(55) Mallia, M. B., Mathur, A., Subramanian, S., Banerjee, S., Kothari, K., Koiry, S. P., Sarma, H. D., and Venkatesh, M. (2006) Synthesis and evaluation of ether containing ^{99m}Tc−nitrido dithiocarbamate complexes as brain perfusion imaging agent. *Appl. Radiat. Isot. 64*, 361−367.
(56) Pasqualini, R., and Duatti, A. (1992) Synthesis and characterization of the new neutral myocardial imaging agent [^{99m}TcN(noet)-2](noet =N-ethyl-N-ethoxydithiocarbamato). *J. Chem. Soc., Chem. Commun. 18*, 1354−1355.
(57) Duatti, A., Marchi, A., and Pasqualini, R. (1990) Formation of the TcN multiple bond from the reaction of ammonium pertechnetate with *S*-methyl dithiocarbazate and its application to the preparation of technetium-99m radiopharmaceuticals. *J. Chem. Soc., Dalton Trans. 12*, 3729−3733.
(58) Pasqualini, R., Duatti, A., Bellande, E., Comazzi, V., Brucato, V., Hoffschir, D., Fagret, D., and Comet, M. (1994) Bis (dithiocarbamato) nitrido technetium-99m radiopharmaceuticals: a class of neutral myocardial imaging agents. *J. Nucl. Med. 35*, 334−341.

DOI: 10.1021/bc500583k
Bioconjugate Chem. 2015, 26, 316−328